Supplementary Figure 1

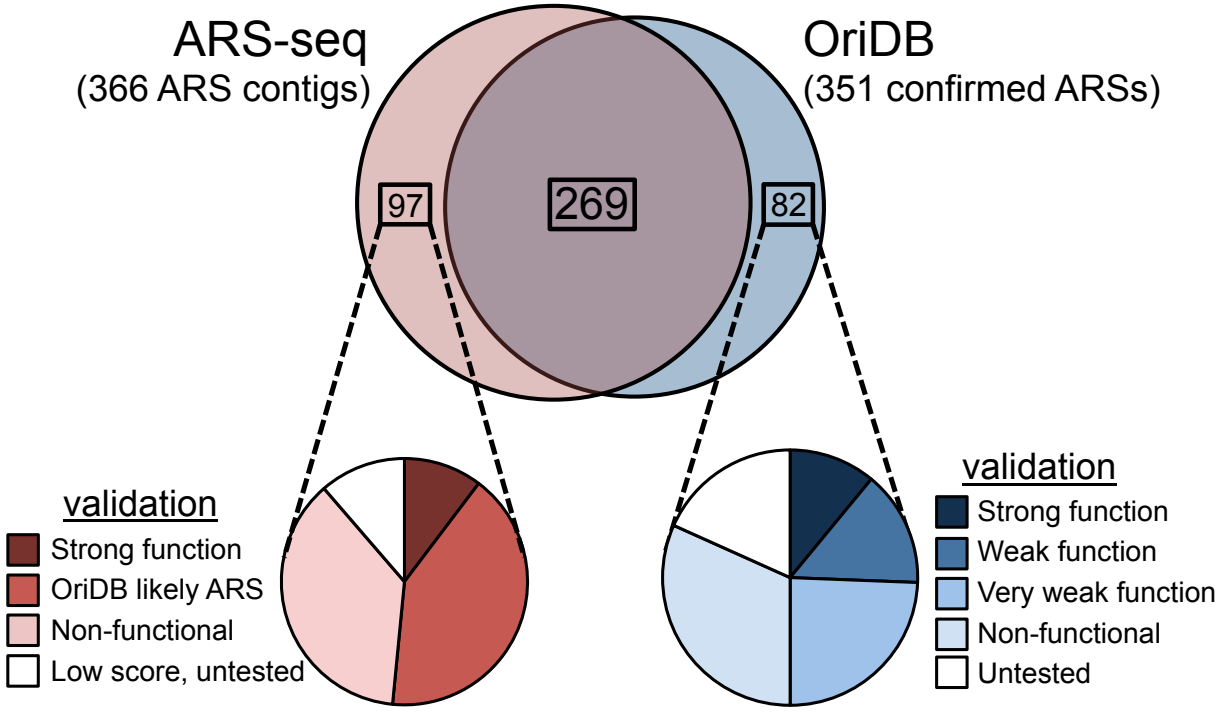

Validation of ARS-seq false positive and false negative candidates and comparison with OriDB. (a) Fragments listed in Supplementary Table 3 and Supplementary Table 4 were cloned into ARS-less vectors, used to transform yeast, and scored for function based on colony sizes relative to control ARS plasmids. Details of filtering and selection of fragments for validation are described in Supplementary Analysis. ARS-seq contigs that did not overlap annotated confirmed ARS regions were validated to remove false positives (left). Categorizations are as follows: strong function: ARS-seq contigs that were tested and found to have ARS function; OriDB likely ARS: ARS-seq contigs that overlapped with likely OriDB ARSs and were presumed to be functional ARSs; Non-functional: contigs that were tested and found to be non-functional; Low score, untested: contigs that had very poor ACS motif matches and were presumed to be non-functional. Annotated OriDB confirmed ARSs that were not captured by ARS-seq were validated to remove false negatives (right). Strong function, Weak function, Very weak function: fragments that showed strong, weak, or very weak ARS function respectively; Non-functional: fragments that were found to be non-functional; Untested: fragments that were not tested.

Supplementary Figure 2

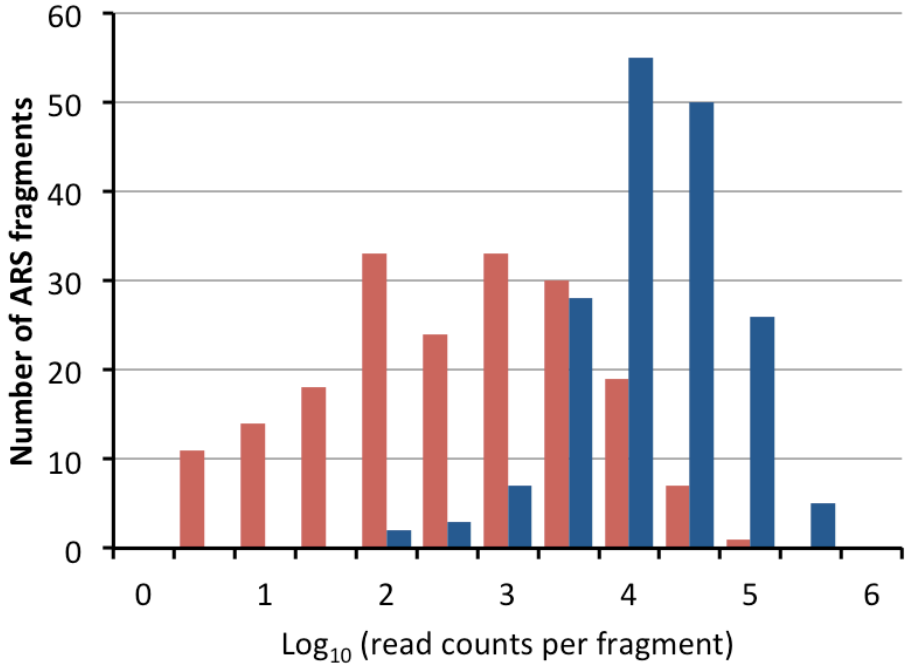

Correlation between ARS-seq read counts and miniARS recovery. The distributions of read counts (log_{10}, x-axis) for ARS-seq contigs overlapped (blue bars) or not overlapped (red bars) by miniARS-seq contigs.

Supplementary Figure 3

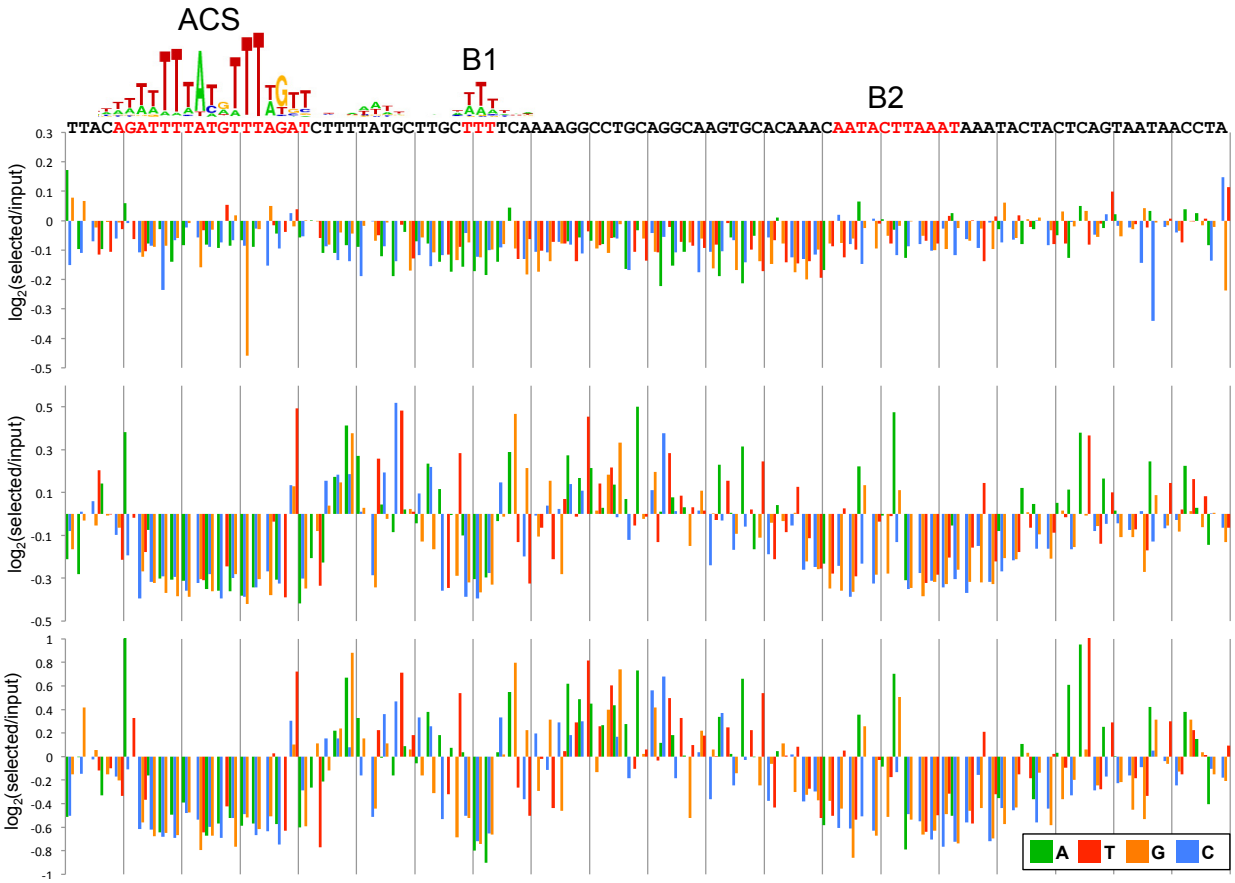

Comparison of mutARS-seq data generated from different samples. (Top chart) ARS1 variant pools generated from sample 1 (0hrs) normalized against variants in the un-transformed plasmid libraries. (Middle chart) Resample 2 (12 hours competitive growth) normalized against resample 1 (0 hours competitive growth). (Bottom chart) Sample 2 (20 hours competitive growth) normalized against Sample 1 (0 hours competitive growth).

Supplementary Figure 4

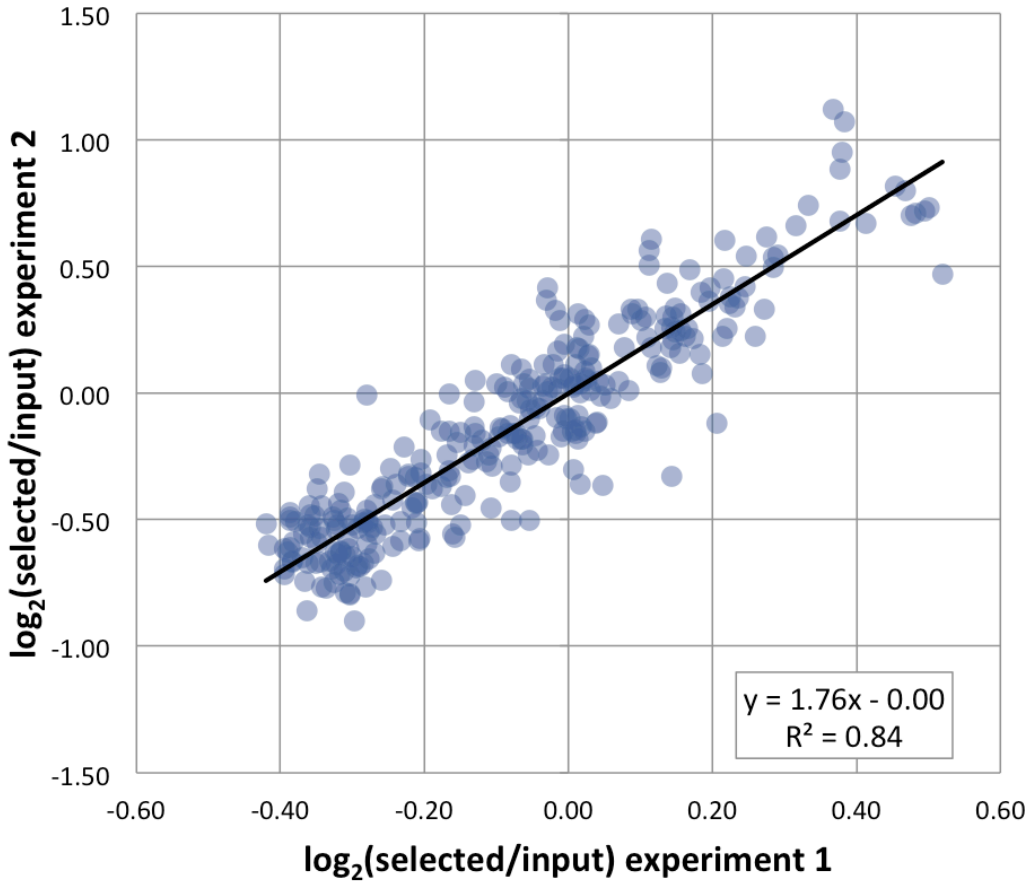

Correlation of enrichment ratios between two separate mutARS-seq experiments (correlation coefficient 0.92). The $\log_2$ transformed ratios of selected/input for each single substitution variant are plotted.

Supplementary Figure 5

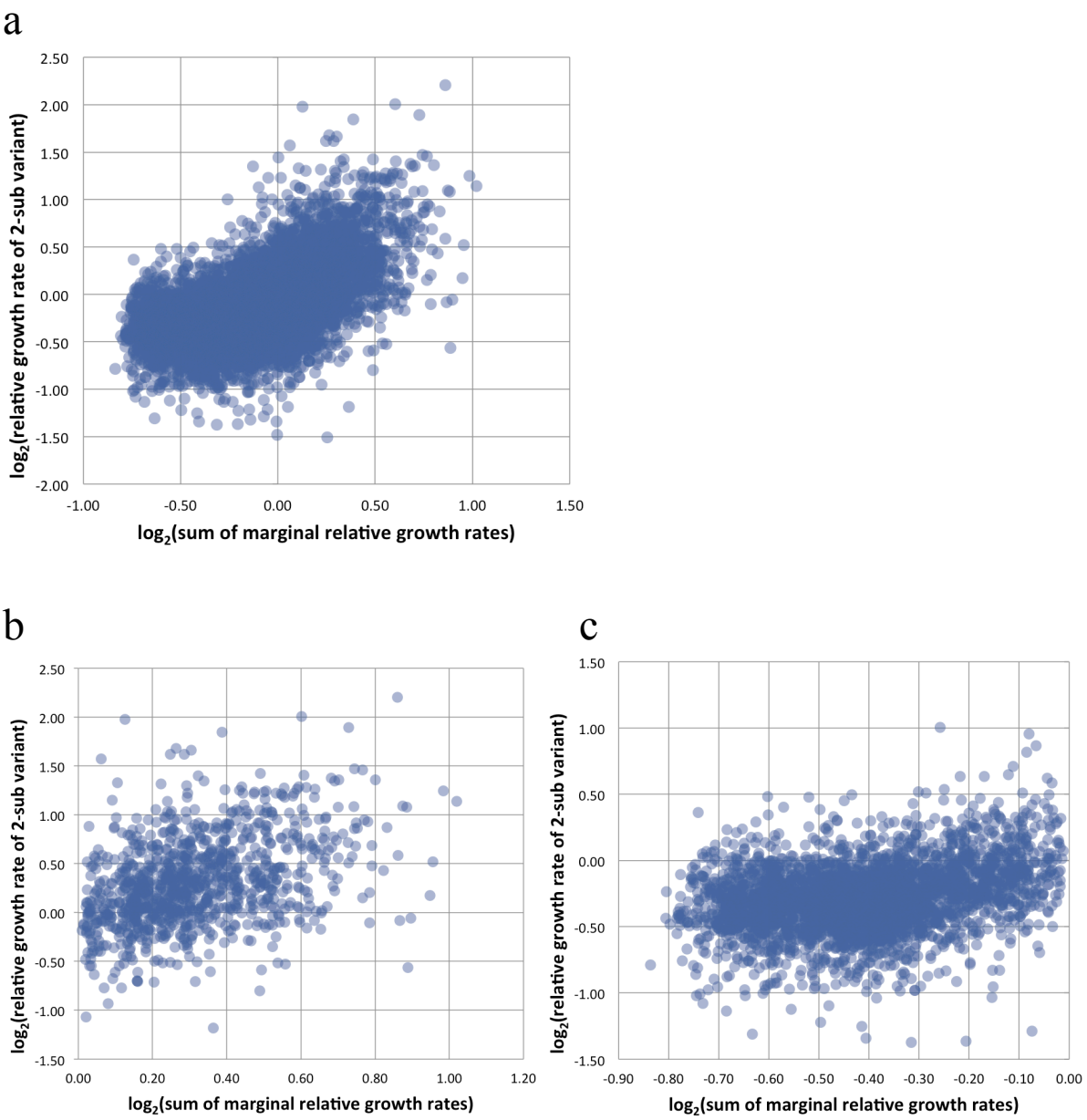

Testing for additive effects in mutARS-seq data. (a) The $\log_2$ enrichment ratios for alleles with two substitutions are plotted as a function of the sum of the enrichment ratios of the two single mutations independently. (b) Same as in (a), except only data for mutations with a positive effect are shown. (c) Same as in (a), except only data for mutations with a negative effect are shown.

Supplementary Figure 6

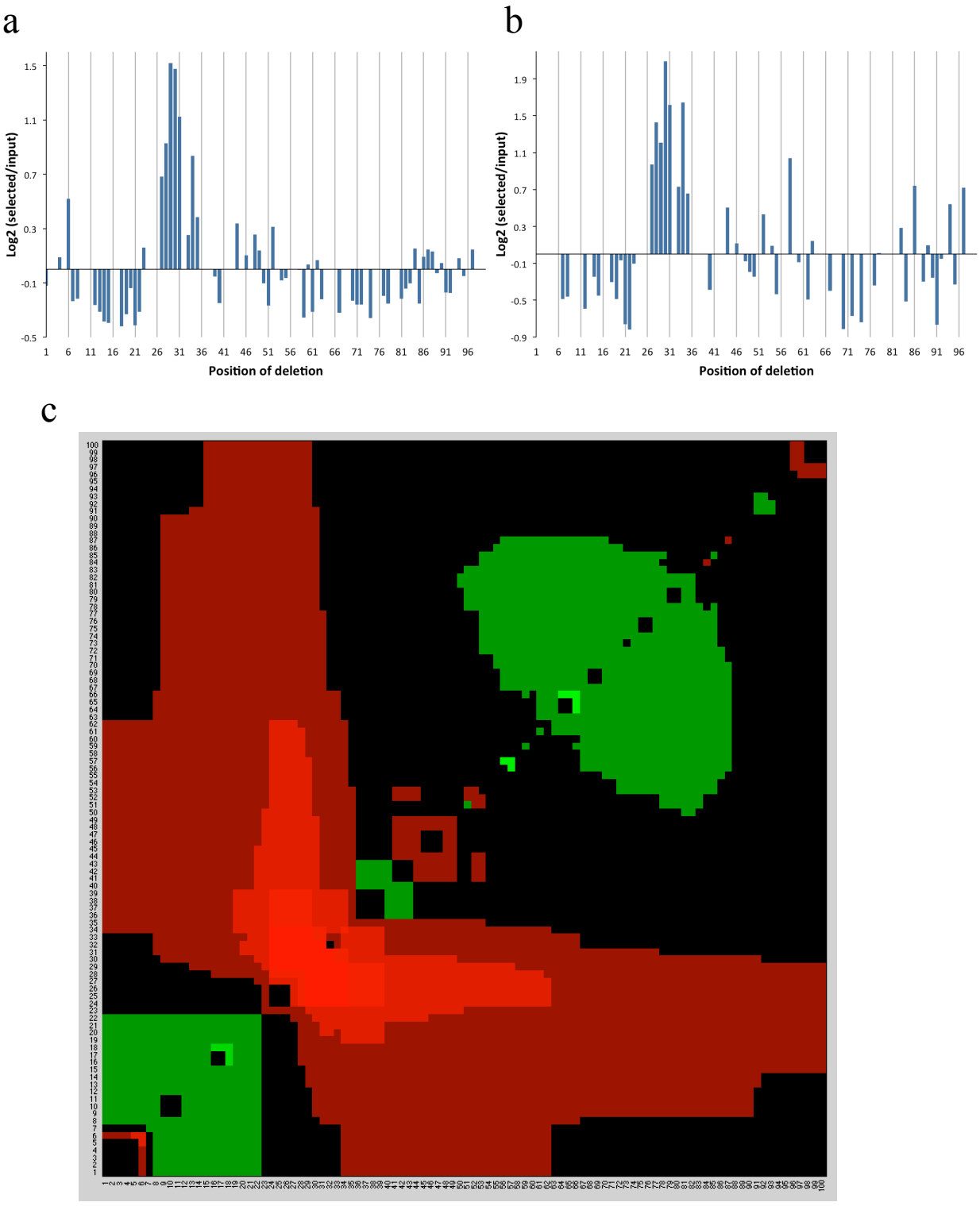

Analysis of mutARS-seq single base deletion variants. (a-b) Log_2 enrichment ratios are plotted as a function of the position of the deletion. Data are shown separately for the 12 hour growth sample (a) and the 20 hour growth sample (b), both normalized against respective sample 1. (c)

Cumulative effects of deletion mutations The (x, y)-entry in this heat map is the $\log_2$ of the WT-normalized ratio between the read pair count in resample 2 and the respective count in resample 1 of all deletions that occur between positions x and y. Red indicates positive entries and green indicates negative ones.

Supplementary Figure 7

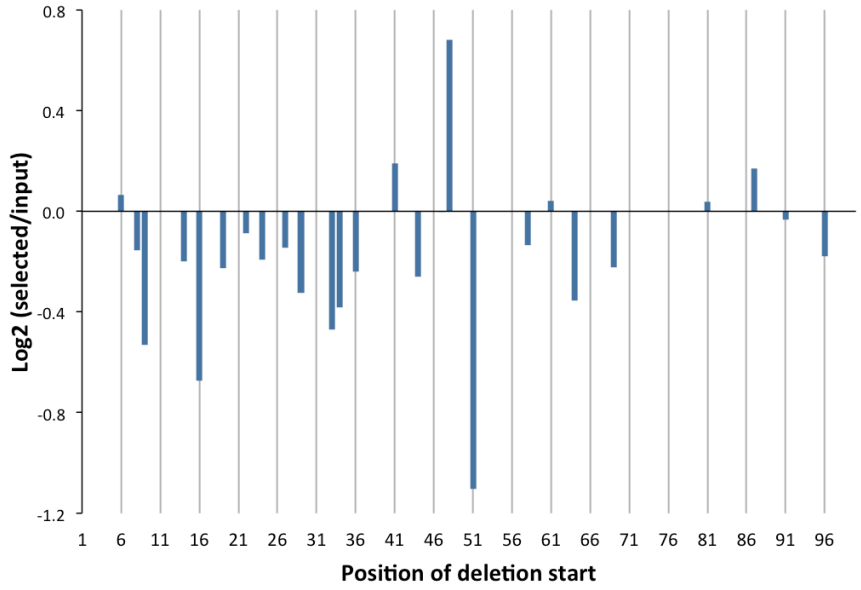

Analysis of mutARS-seq adjacent 2-base deletion variants. Log_2 enrichment ratios are plotted as a function of the position of the start of the 2bp deletion.

Supplementary Figure 8

a

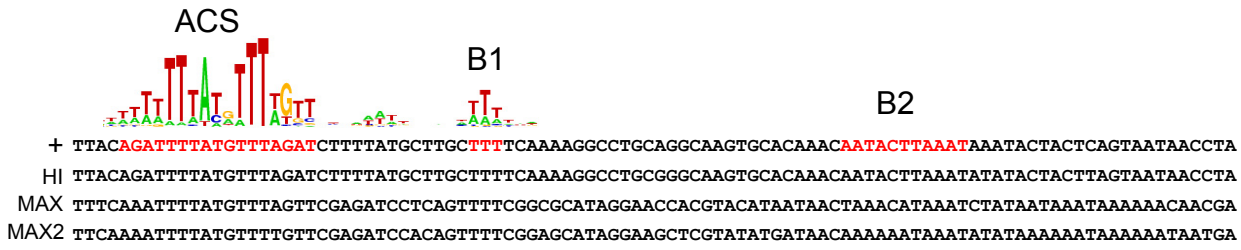

b

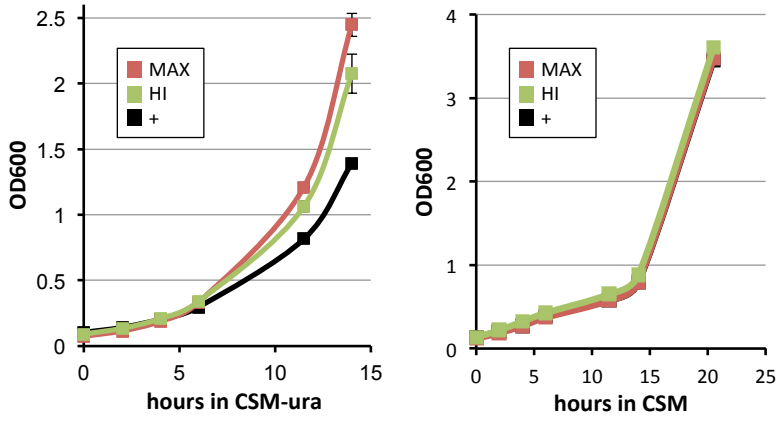

c

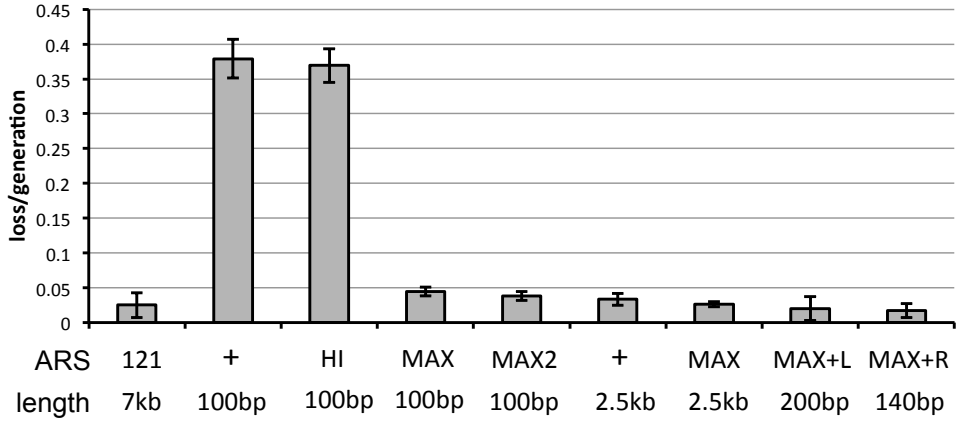

Design and characterization of *ARS1max* sequences. (a) Sequence comparison between *ARS1* (+), *ARS1hi1* - the most efficient allele identified by mutARS-seq (HI) and two *ARS1max* sequences each designed from a different mutARS-seq experiment (MAX - *ARS1max*; MAX2 - *ARS1max2*). *ARS1max* was designed using data from mutARS-seq experiment Sample 2 (Figure 2, Supplementary Figure 3, bottom chart) and *ARS1max2* was designed using mutARS-seq

experiment Re-sample 2 (Supplementary Figure 3, middle chart). (b) Growth curves in CSM-uracil and CSM of strains bearing indicated ARS plasmids. (c) Plasmid loss measurements in wildtype yeast using different ARSs (121 - control *ARS121*; + - *ARS1*; HI - *ARS1hi1*; MAX - *ARS1max*; MAX2 - *ARS1max2*). To test the effect of adding flanking *ARS1* DNA to *ARS1max* we designed and tested MAX+L (ARS1max + 100bp of endogenous flanking DNA to the left on the T-rich strand) and MAX+R (ARS1max + 40bp of endogenous flanking DNA to the right on the T-rich strand, which captures the previously described B3 element).

Supplementary Figure 9

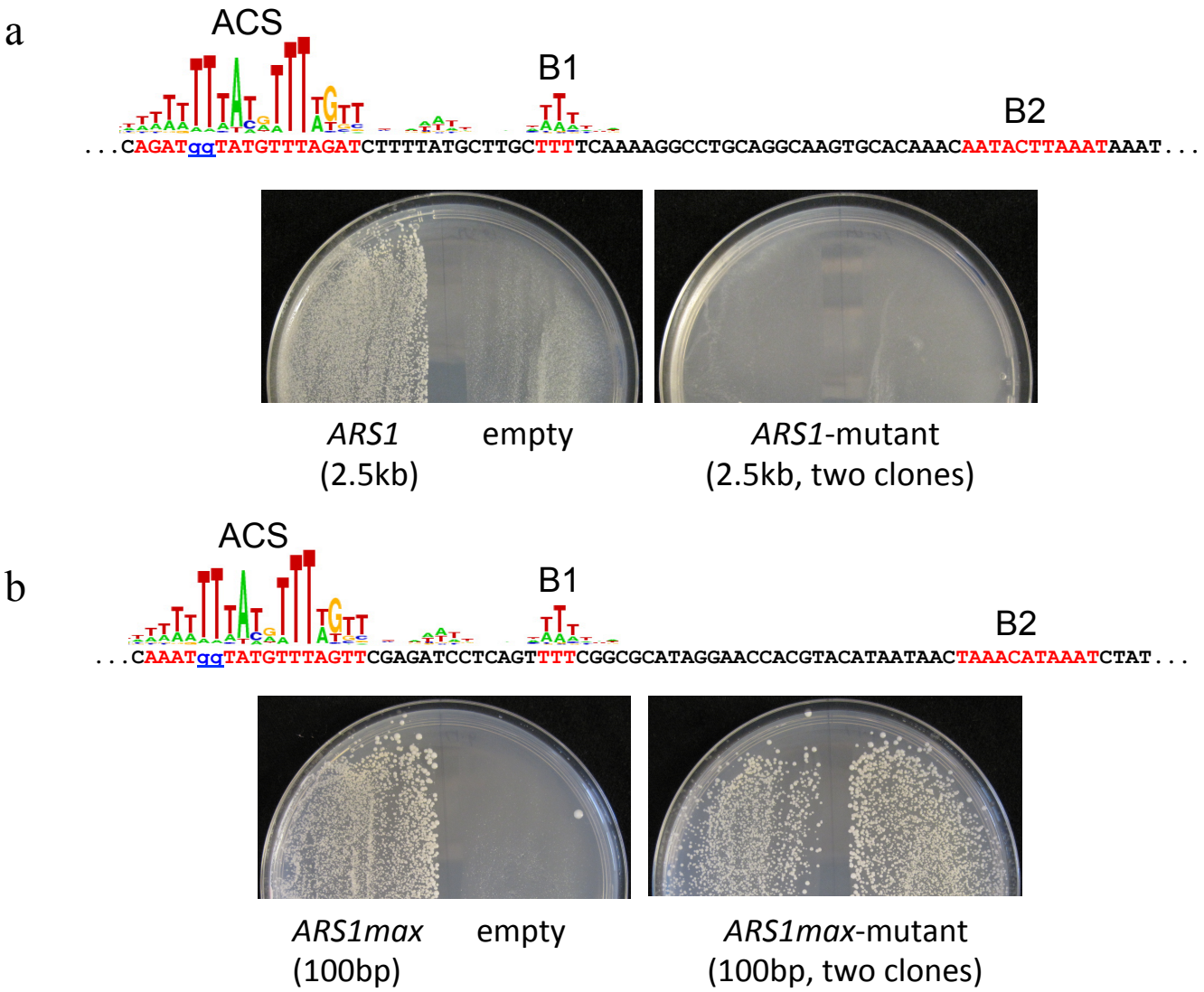

The function of *ARS1max* is not dependent on the primary ACS. We used site directed mutagenesis to construct mutant alleles of *ARS1*(a) and *ARS1max* (b) where a TT di-nucleotide in the ACS was replaced by a GG di-nucleotide (indicated in blue). The ARS assay indicates that while *ARS1* requires the ACS for function (a, two independent plasmid isolates shown in the lower right panel), the *ARS1max* mutant allele retains function, suggesting that *ARS1max* does not require the original ACS for function. The mutations were introduced into a 100bp allele of *ARS1max* and into a 2.5kb fragment of *ARS1* to compensate for the lower activity of the wildtype *ARS1* allele.

Supplementary Figure 10

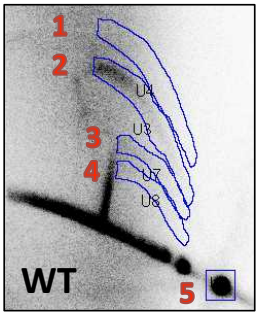

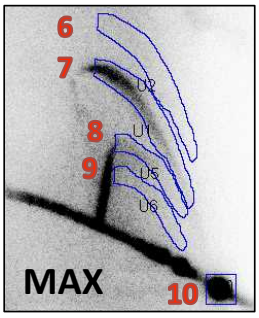

Area	Description	Signal #1	Normalized #1	Signal #2	Normalized #2
2	WT bubble-arc	59278	19723	8370	1721
1	background in 2	39555		6649	
3	WT Y-arc	17962	1221	4017	101
4	background in 3	16741		3916	
5	WT non-replic.	85144		N/A	
7	MAX bubble-arc	82247	45093	15331	5373
6	background in 7	37154		9958	
8	MAX Y-arc	27348	928	6155	133
9	background in 8	26420		6022	
10	MAX non-replic.	247346		N/A	
		Y/Bubble WT	0.062		0.059
		Y/Bubble MAX	0.021		0.025

Quantification of 2D gel signal. The probed membranes were scanned using the Quantity One v. 4.6.9 software on the Personal Molecular Imager (BioRad). Radioactive signal was measured by selecting identically shaped areas that encompass the bubble arcs (labelled 2 and 7 above) and in areas very close to the bubble-arcs to measure background (labelled 1 and 6 above). Similar analysis was performed to quantitate signal and background for Y intermediates in the ascending arm of the Y-arcs (areas 3, 4, 8, 9 above). Two replicate experiments were performed (#1 and #2 in the table above, only scans for replicate #1 are shown). The signal measurements are provided in the table above (Signal #1 and Signal #2 correspond to both replicates). To generate the Y/ Bubble ratios for *ARS1* (WT) and *ARS1max* (MAX) we subtracted the signal of a given background area from the relevant arc area (Normalized #1 and #2) and then divided the normalized Y-arc signal by the normalized bubble-arc signal. The ratios are indicated in the lower portion of the table. Our data show that while in the wildtype *ARS1* strain 5.9%-6.2% of the selected replicating intermediate signal comes from the Y-arcs, in the *ARS1max* strain 2.1%-2.5% of the signal comes from the Y-arcs. The fraction of replicating intermediates can be estimated by taking the ratio of combined arc signals to the non-replicating 1N spot on the gel (non-repl.). In the experiment shown both WT and MAX samples have comparable signals of total intermediates (24% and 18% respectively). These measurements indicate that origin firing is increased in the *ARS1max* strain.